Bull. Mater. Sci. (2022) 45:124
https://doi.org/10.1007/s12034-022-02710-8

Prediction study of the structural, elastic, electronic, dynamic, optical and thermodynamic properties of cubic perovskite $BiGaO_3$

M A GHEBOULI[1,2], B GHEBOULI[3], L KRACHE[4], SULTAN ALOMAIRY[5], M FATMI[2,*], T CHIHI[2] and M REFFAS[2]

[1]Department of Chemistry, Faculty of Technology, University of Mohamed Boudiaf, 28000 M'sila, Algeria
[2]Research Unit on Emerging Materials (RUEM), University of Setif 1, 19000 Sétif, Algeria
[3]Laboratory of Studies Surfaces and Interfaces of Solids Materials, Department of Physics, Faculty of Science, University Ferhat Abbas of Setif 1, 19000 Sétif, Algeria
[4]PQSD Laboratory, Department of Physics, Faculty of Science, University Ferhat Abbas of Setif 1, 19000 Sétif, Algeria
[5]Department of Physics, College of Science, Taif University, P.O. Box 11099, Taif 21944, Saudi Arabia
*Author for correspondence (fatmimessaoud@yahoo.fr)

MS received 12 October 2021; accepted 13 March 2022

Abstract. Some fundamental physical properties of $BiGaO_3$ were investigated under pressure and temperature effect using GGA and LDA. The effect of orientation on Debye temperature and sound wave velocities were estimated from elastic constants. The bulk modulus value of $BiGaO_3$ is a sign of its high hardness, because it is linked to an isotropic deformation. $BiGaO_3$ is a semiconductor and ductile material, with covalent (Ga–O) and ionic Bi-O bonding. The optical transitions were observed when electrons pass from the top of the valence band (O-2p) to the bottom of the conduction band (Ga-4p or Bi-6p). The thermodynamic parameters were determined in temperature and pressure ranging from 0 to 1800 K and 0 to 50 GPa.

Keywords. $BiGaO_3$ perovskite; optical absorption; first principle; band structure.

1. Introduction

The researchers were particularly interested in perovskite oxides for their applications as ferroelectric, piezoelectric and multiferroic [1–3]. The used materials in ferroelectric and piezoelectric devices are lead-based compounds and toxic. Therefore, it is necessary to look for a new material as a replacement that shows the same characteristics but less harmful for the environment. The search and development of such alternative piezoelectric materials is now a very active topic research and leads on bismuth-layer structure. Bismuth layer structure possess a high Curie temperature, high mechanical quality factor, large dielectric breakdown strength, good aging characteristics and good piezoelectric properties, which make them candidate materials for ceramic filter and resonator applications. Bi-based compounds are the most candidates as individual lead-free piezoelectric because they are nontoxic and have $6s^2$ lone pairs, which is the origin of large ferroelectric polarizations [4,5]. The perovskite bismuth gallate $BiGaO_3$ (Ga is nonmagnetic ion) crystallized in the cubic, hexagonal, tetragonal and orthorhombic structure. Experimental results show that $BiGaO_3$ crystallizes in the orthorhombic structure at ambient pressure. The structural, elastic and electronic properties of $BiGaO_3$ compound have been carried out for the ideal cubic [6,7] and orthorhombic structures [8–10]. Bismuth gallate $BiGaO_3$ was experimentally synthesized using high pressure at high temperature [11]. The experimental investigation [12,13] on the physical properties of bulk and nanostructure of these compounds are limited compared to other multiferroic material. Piezoelectric materials are widely used for the applications in actuator, sensor, energy-storage and energy-harvesting devices [14]. $BiGaO_3$ is one of the most efficient compound to tune the expansion behaviour [15]. Bismuth gallium oxide is a typical perovskite ferroelectric, which has a large ferroelectric polarizations and piezoelectric responses [16]. $BiGaO_3$ undergoes a pressure-induced first-order phase transition from pyroxene to monoclinic at 3.5 GPa, and then to rhombohedral at 5.2 GPa, and finally to orthorhombic structure at 7.4 GPa [17]. The compound $BiGaO_3$ is suitable candidate co-dopant for further control of phase boundary structure [18]. Bi-containing perovskites and perovskite-related materials such as $BiGaO_3$ have received a lot of attention as lead-free ferroelectric material [12].

In this work, we focus on the detailed study of structural, elastic, electronic, optical and thermodynamic properties of cubic bismuth gallate $BiGaO_3$ within GGA and LDA using

Published online: 02 July 2022

the plane wave pseudo-potential method of the density functional theory.

2. Computational method

Computations were carried out using CASTEP code [19]. Kohn–Sham equations were treated by density functional theory framework [20,21], where wavefunctions of valence electrons have smaller kinetic energy cut-off. Vanderbilt-type ultra soft pseudo-potential [22] represent the interaction of valence electrons with ion cores. The GGA of Perdew *et al* [23], LDA of Goedecker *et al* and Pade parameterization [24] are adopted for the exchange-correction functional. The discrete summation over k-points scheme of Monkhorst–Pack [25] replaces integrations in the Brillouin zone. The cut-off energy of 660 eV with k-points 8 × 8 × 8 ensures well convergence of structure and energies. The computation of optical parameters requires the use of 20 × 20 × 20 uniform k-points. The structural parameters were determined using Broyden-Fletcher-Goldfarb-Shanno minimization technique [26]. The tolerance of geometry optimization was total energy 5×10^{-6} eV per atom, maximum ionic Hellmann-Feynman force 10^{-2} eV $Å^{-1}$ and maximum stress 2×10^{-2} eV $Å^{-3}$. The quasi-harmonic Debye model is used in thermal effect to describe the variation $E(V)$ [27]. Gibbs program evaluates Debye temperature, obtains G (P, V, T) and minimize it and derives V (P, T). Detailed description of this model is found in [28–31].

3. Results and discussion

3.1 *Ground state properties*

The $BiGaO_3$ perovskite is modelled in the ideal cubic structure. The unit cell consists of unit formula with Wyckoff positions of the atoms Bi:1a (0, 0, 0), Ga:1b (1/2, 1/2, 1/2) and O:3c (1/2, 1/2, 0). The electronic configuration of Bi, Ga and O atoms is Bi: [Xe] $4f^{14}$ $5d^{10}$ $6s^2$ $6p^3$, Ga: [Ar] $3d^{10}$ $4s^2$ $4p^1$ and O: $1s^2$ $2s^2$ $2p^4$. The behaviour of the structural parameters of $BiGaO_3$ under pressure requires knowledge of the cell geometry at a pressure ranging from 0 to 40 GPa. The pressure as a function of normalized volume is visualized in figure 1, with respect to the fit Murnaghan [32]. The computed lattice parameters are listed in table 1. Our GGA structural parameters are closer to previous calculations carried out within the Wien2k computer code [33]. The LDA value of lattice constant (bulk modulus) is lower (greater) than that given by GGA. In a cubic structure, the bulk modulus is a good indicator of hardness because it is linked to isotropic deformation. The results show that $BiGaO_3$ has high bulk modulus, which is a sign of strong hardness.

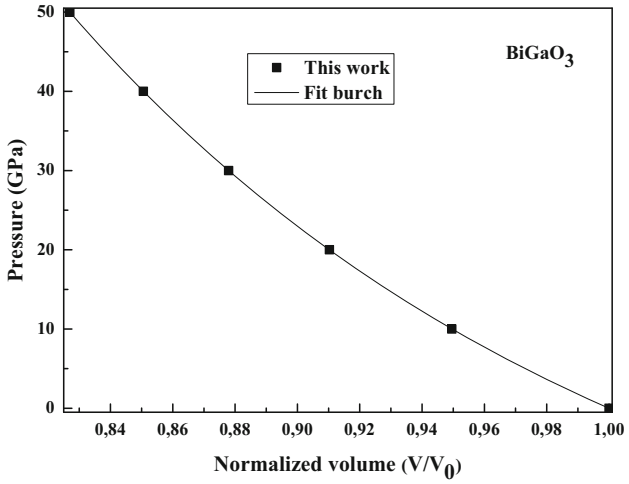

Figure 1. The pressure dependence on normalized volume for $BiGaO_3$.

3.2 *Elastic constants*

The elasticity of $BiGaO_3$ is described using three independent parameters C_{11}, C_{12} and C_{44}. We estimated them by determining the stress tensor under application of strain. The knowledge of elastic constants detect the binding between adjacent atoms, the anisotropy of bond and stability. The elastic moduli of $BiGaO_3$ determined by perturbation method at equilibrium pressure within GGA and LDA are listed in table 2. It seems that our elastic constants are closer to other computation carried out within Wien2k computer code [33]. The elastic moduli computed by LDA are greater than those determined within GGA. Equation (1) represents the computed elastic moduli of $BiGaO_3$ are positive and satisfying the following conditions to ensure their elastic stability [34]:

$$C_{11} + 2C_{12} \rangle 0, C_{44} \rangle 0, C_{11} - C_{12} \rangle 0, C_{12} \langle B \langle C_{11} \quad (1)$$

The calculated bulk modulus from elastic constants is closer to that given by fit Murnaghan. This proves our accurate calculation of elastic constants. The evolution of elastic moduli under pressure effect is shown in figure 2. This compound has high elastic moduli, and then strong hardness. The elastic moduli of $BiGaO_3$ increase monotonously with increasing pressure, furthermore the variation on C_{44} is a little sensitive to the pressure. The elastic constants allow us to obtain the parameters listed in table 3 using Voigt [35], Reuss [36] and Hill [37]

Table 1. Lattice constant, bulk modulus and its pressure derivative calculated from Birch for $BiGaO_3$ perovskite.

Material	Approach	Refs.	a (Å)	B_0 (GPa)	B'
BiGaO3	GGA	This work	3.8988*	172.74*	4.40*
	LDA	Exp.	3.8147*	215.21*	4.38*
		Other	3.899 [33]	206.87 [33]	

*From Birch.

Table 2. Computed elastic moduli, bulk modulus calculated from elastic constants and its pressure derivative of $BiGaO_3$ perovskite.

Material	Approach	Refs.	C_{11}	C_{12}	C_{44}	B_0	B'	Θ_D
BiGaO3	GGA	This work	279.52	115.79	92.31	170.37	4.06**	450.76
	LDA	Exp.	355.03	145.30	105.51	215.21	4.01**	489.53
		Other	292.19 [33]	115.08 [33]	96.73 [33]	170.99 [33]		

**From elastic constants.

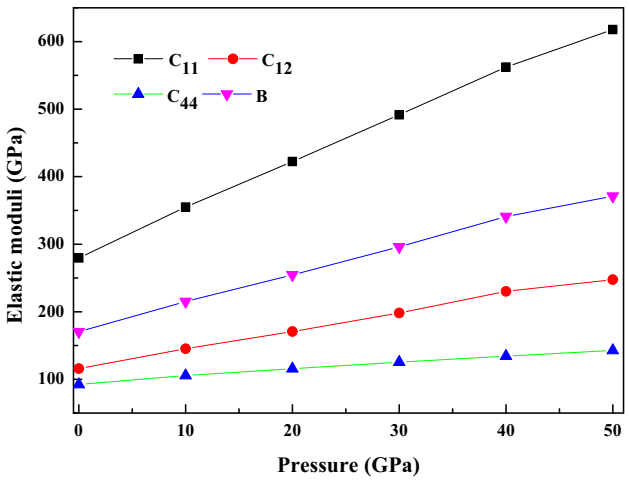

Figure 2. Plots of elastic moduli as a function of pressure for $BiGaO_3$.

approximations. The Poisson's ratio of $BiGaO_3$ is closer to the limit value 0.25, so the Bi-6p and O-2p states bonding is ionic [38]. The anisotropy factor value indicates that $BiGaO_3$ is isotropic. The greater B_H/G_H ratio value than 1.75 traduces the ductility of $BiGaO_3$. We visualize in figure 3 the directional dependent of Poisson's ratio, shear modulus, linear compressibility and Young modulus in 3D dimensions using ELATE software [39]. The spherical shape translates the isotropic material. From figure 3, we note that linear compressibility and Young's modulus are practically isotropic, while Poisson's ratio is anisotropic and little anisotropy is observed in shear modulus of $BiGaO_3$. The predicted maximum and minimum values of directional dependent are listed in table 4.

3.3 *Debye temperature*

Debye temperature is obtained from elastic data using the mean sound velocity and mean atomic volume. The method of calculation for Debye temperature and sound wave velocities from elastic constants is found in references [40–42]. The computed Debye temperature of $BiGaO_3$ is listed in table 2. The value given by the LDA exceeds that

Table 3. Bulk modulus, shear modulus, Young's modulus, Poisson's ratio and anisotropy factor for $BiGaO_3$.

	B			G						
Material	B_v	B_R	B_H	G_v	G_R	G_H	E_H	σ_H	A^U	B_H/G_H
$BiGaO_3$										
GGA	170.37	170.37	170.37	88.13	87.83	87.98	225.18	0.279	0.017	1.93
LDA	202.01	202.01	202.01	104.99	104.97	104.98	268.44	0.278	0.001	1.92

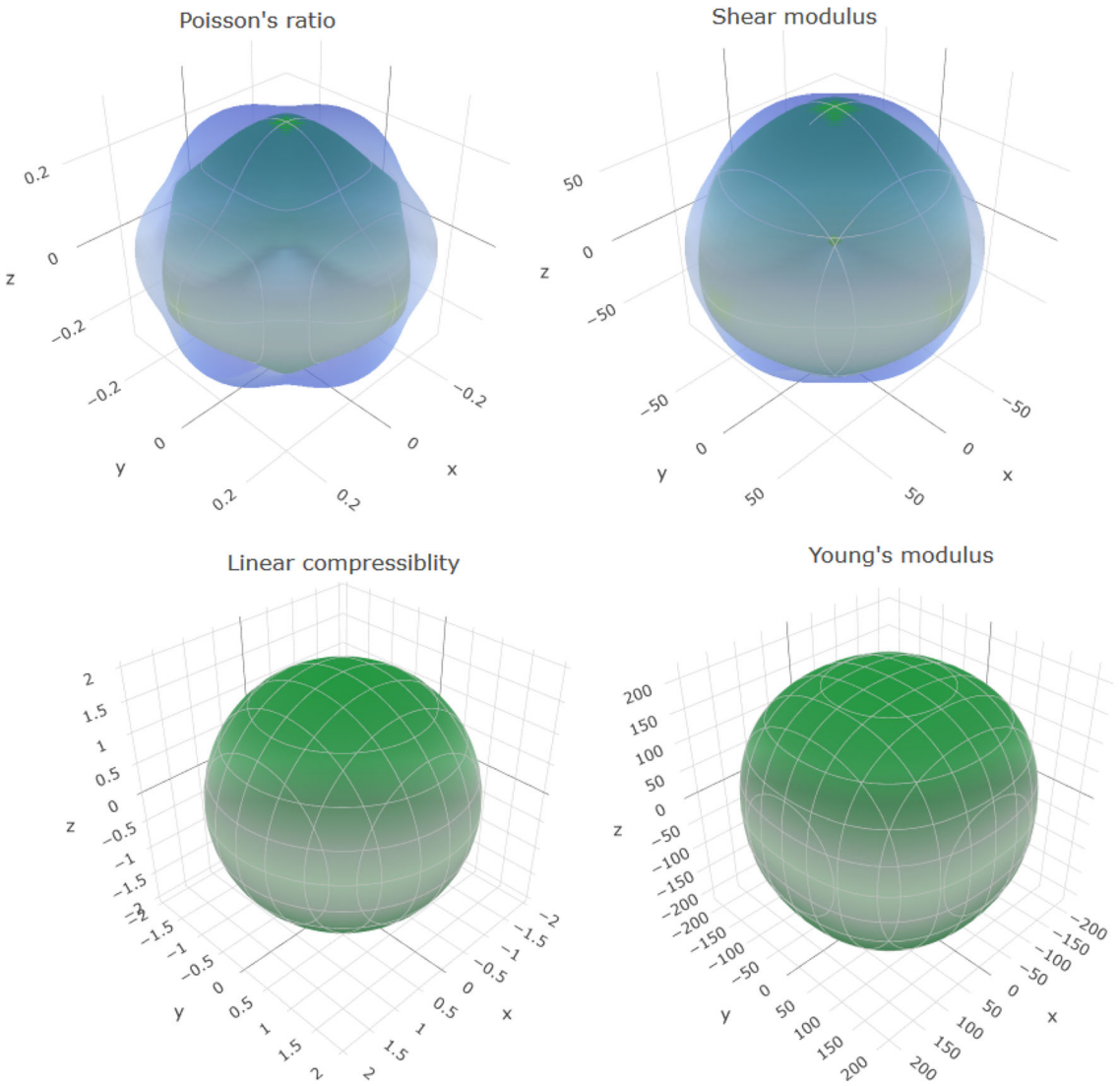

Figure 3. The orientation effect on Poisson's ratio, shear modulus, linear compressibility and Young's modulus for $BiGaO_3$.

Table 4. Predicted maximum and minimum values of directional-dependent Young's modulus, linear compressibility, shear modulus and Poisson's ratio for $BiGaO_3$.

	Young's modulus		Linear compressibility		Shear modulus		Poisson's ratio	
	E_{min}	E_{max}	β_{min}	β_{max}	G_{min}	G_{max}	σ_{min}	σ_{max}
$BiGaO_3$								
GGA	211.69	234.5	1.9565	1.9565	81.866	92.317	0.23708	0.31604
LDA	264.4	271.17	1.6501	1.6501	103.13	106.24	0.26816	0.28724

carried over by the GGA. We predicted the elastic wave velocities of $BiGaO_3$ along [100], [110], [111] and [001] directions using GGA in table 5. The GGA and LDA longitudinal (shear) waves are fastest (slowest) along [111] direction for $BiGaO_3$.

3.4 *Electronic properties*

We show in figure 4 the electronic band structures along high symmetry Γ, R, M and X points for $BiGaO_3$ at equilibrium lattice constant using GGA and HSE06,

Table 5. Calculated elastic wave velocities along [100], [110], [111] and [001] directions for $BiGaO_3$.

		[100]		[110]		[111]	
Material	Direction	GGA	LDA	GGA	LDA	GGA	LDA
$BiGaO_3$	V_L (m s^{-1})	3621	3747	3932	4182	4031	4317
	V_{T1} (m s^{-1})	2689	2758	3123	2883	2379	2303
	V_{T2} (m s^{-1})	2689	2758	2689	2758	2379	2303

taking into account also the spin-polarized effect. The use of the HSE functional improves the results given by the GGA, which is intended for the study of the fundamental state and does not take into account the effect of excitation. The bandgap in $BiGaO_3$ is indirect type (M→X) with values 1.015, 1.144 and 1.893 eV for GGA, spin polarized and HSE functional, respectively. It can be seen that the HSE functional gives a value in good agreement with the experimental value 1.88 eV reported in the literature calculated with GGA-PBE using Vienna *ab initio* Simulation Package. The valence band is grouped into three distinct regions with energy range –20 to E_F. The two upper valence bands are at (–8.25 eV to E_F) and (–12.75 to –9.08 eV). The first occupied conduction band is situated at (1.25 to 5.45 eV). We plot in figure 5 the effect of pressure on direct and indirect bandgaps between various symmetry points. One can notice that all energy gaps increase monotonously with increasing pressure. The fundamental E_{M-X} and E_{R-X} indirect energy gap plotted in figure 6 increases monotonously with increasing pressure and changes from E_{M-X} to E_{R-X} at about 25 GPa. Total and partial densities of states as shown in figure 7 indicate that O-2p sites and small participation of Ga-4p and Bi-6p states occupy the upper valence band. The first conduction band located between E_F and 2.39 eV is empty. Then transition occurs between O-2p and Bi-6p or Ga-4p. The hybridization of Ga-4p orbital with O-2p site close to the Fermi level implies that Ga–O bond has a covalent bonding character. There is also small contribution from Bi-6p state. However, Bi-6p state is dominating at the conduction band minima, which proves the ionic bonding nature of Bi-O bond.

3.5 *Phonon frequencies*

The term 'phonon' means a quasi-particle associated with a progressive elastic wave. The vibrations are treated in terms of norm-modes for optical or acoustical phonon frequencies and longitudinal or transversal propagation. We computed phonons dispersion curves by density functional perturbation theory. The phonons dispersion curves for $BiGaO_3$ are visualized in figure 8. We point out that the main features of phonons dispersion spectra are the following:

(1) Longitudinal optical are separated by a frequency gap 25 cm^{-1}.
(2) The maximum of longitudinal (acoustical) branches is located between R (at Γ and X) points.
(3) There is an overlap between longitudinal and transversal acoustical branches.
(4) There are soft modes in this semiconducting material.
(5) The soft modes indicate the existence of more stable phases such as, phase Pcca (orthorhombic) and phase R3c (trigonal).

3.6 *Optical properties*

The Bi atom is heavy, so the spin-polarized effect is important in the study of optical properties and gives results that are more reliable. The study of transitions from five upper valence bands to five lower conduction bands requires the knowledge of imaginary part of dielectric function with and without spin-polarized effect, which we display in figure 9. The shape of the imaginary part of the dielectric constant is similar with and without spin-polarized effect. However, the peaks are more intense in the absence of the spin effect. The dielectric function, $\varepsilon(\omega)$, is a fundamental optical parameter that describes the absorption and polarization properties of the material, where $\varepsilon_1(\omega)$ and $\varepsilon_2(\omega)$ are, respectively, the real and imaginary part of the dielectric function. From equation (2), the imaginary part $\varepsilon_2(\omega)$ can be obtained from the momentum matrix between the occupied and unoccupied electronic states, which is given by [43]:

$$\varepsilon_2(\omega) = \frac{2\omega^2\pi}{V\varepsilon_0}\sum_{k,v,c} |<\psi_k^c|\mathbf{u}.\boldsymbol{r}|\psi_v^c>|^2\delta\left(E_k^c - E_k^v - \hbar\omega\right) \tag{2}$$

where **u** is the vector that provides the polarization of the electric field of the incident electromagnetic radiation, V is the volume of the unit cell, e the electronic charge and ψ_k^c represents the wavefunction of the valence (conduction) band at the wave vector k. From equation (3), the real part $\varepsilon_1(\omega)$ of the dielectric function $\varepsilon(\omega)$ is calculated from the imaginary part of $\varepsilon_2(\omega)$ according to Kramers–Kronig relations [44]:

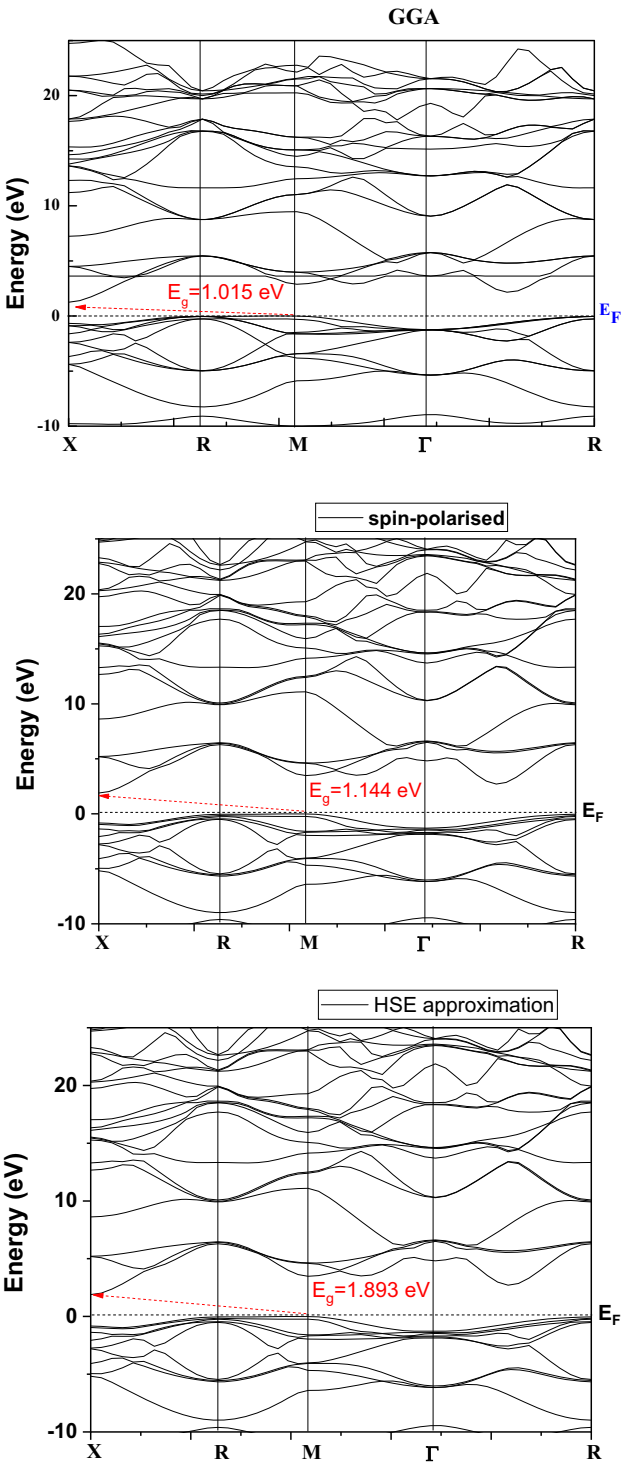

Figure 4. The band structure of $BiGaO_3$ at X, R, M and Γ symmetry points in the Brillouin zone.

$$\varepsilon_1(\omega) = 1 + \frac{2}{\pi} P \int_0^{\infty} \frac{\omega' \varepsilon_2(\omega')}{\omega'^2 - \omega^2} \mathrm{d}\omega' \tag{3}$$

where P implies the principal value of the integral.

Transition energy $E(k) = E_{cj}(k) - E_{vi}(k)$ is plotted in figure 10; where v_i and c_j are the level of valence and

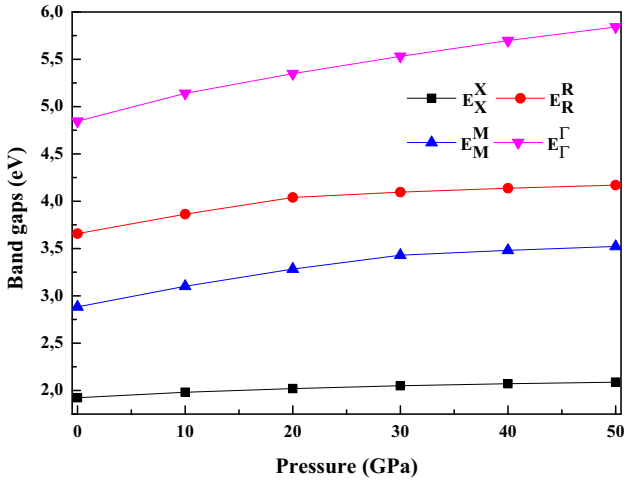

Figure 5. The effect of pressure on direct and indirect bandgaps for $BiGaO_3$.

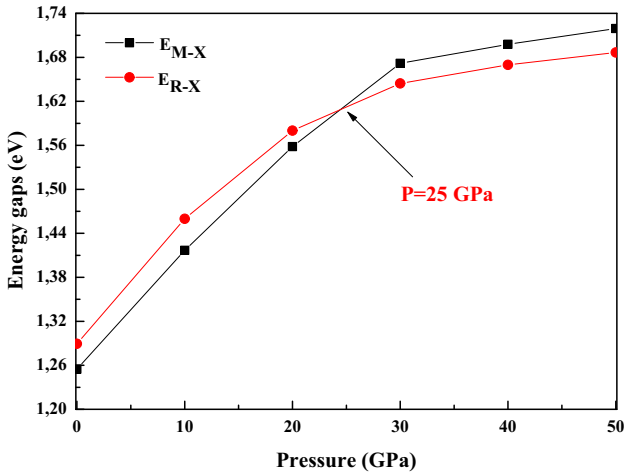

Figure 6. The fundamental bandgap *vs.* pressure.

conduction bands. The imaginary part threshold energy occurs at 1.65 eV, which is the fundamental indirect bandgap of $BiGaO_3$. We study transitions from occupied O-2p orbital to unoccupied Bi-6p or Ga-4p site. The peak with energy 3.55 eV corresponds to transitions V_1-C_2 at M point, (V_1-C_1, V_2-C_1 or V_3-C_1) at R point or V_5-C_1 at X point. The second structure centred at 4.82 eV originates mainly from transitions V_1-C_1, V_2-C_1, V_4-C_1, V_1-C_2, V_5-C_2, V_4-C_2, V_5-C_1 at Γ point. For energy 6.82 eV, $BiGaO_3$ exhibits V_5-C_3, V_5-C_4 at X point and V_5-C_5, V_4-C_5, V_3-C_5, V_4-C_4, V_5-C_4, and V_3-C_3 transitions located near Γ point. Transitions V_2-C_5, V_4-C_5, V_5-C_5 can be observed at R point for energy 8.96 eV. Energy 11.85 eV is origin of V_5-C_5 transition positioned between M and R points. We plot the loss function spectra with and without spin-polarized effect *vs.* wavelength for $BiGaO_3$ in figure 11. Spin-polarized is reported to reduce energy losses. We distinguish the high loss energy in the range 36.55 to 51 nm,

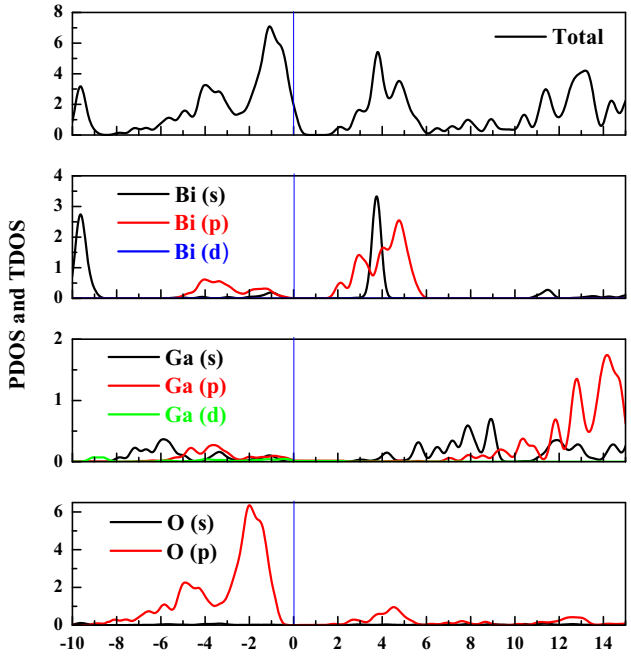

Figure 7. The total (TDOS) and partial (PDOS) densities of states for $BiGaO_3$.

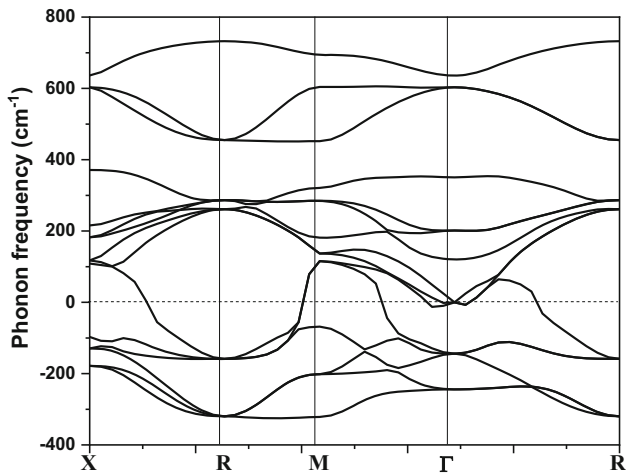

Figure 8. The phonon frequencies for $BiGaO_3$.

which changes wavelength after the ionization edge. The lower loss energy corresponds to wavelength less than 36.55 nm and greater than 51 nm and can provide information about composition and electronic structure. The loss function reaches the maximum value 8.81 at 42.3 nm for $BiGaO_3$. The reflectivity with and without spin-polarized effect of $BiGaO_3$, as shown in figure 12, has a value 0.019, which corresponds to wavelength 31.9 nm. There is less reflectivity with spin-polarized. After successive aggrandizement, it reaches a maximum value of 0.64 at 43 nm. The absorption peaks with and without spin-polarized effect, as depicted in figure 13, are attributed to the phototransition energies from maximum valence band to minimum conduction band under

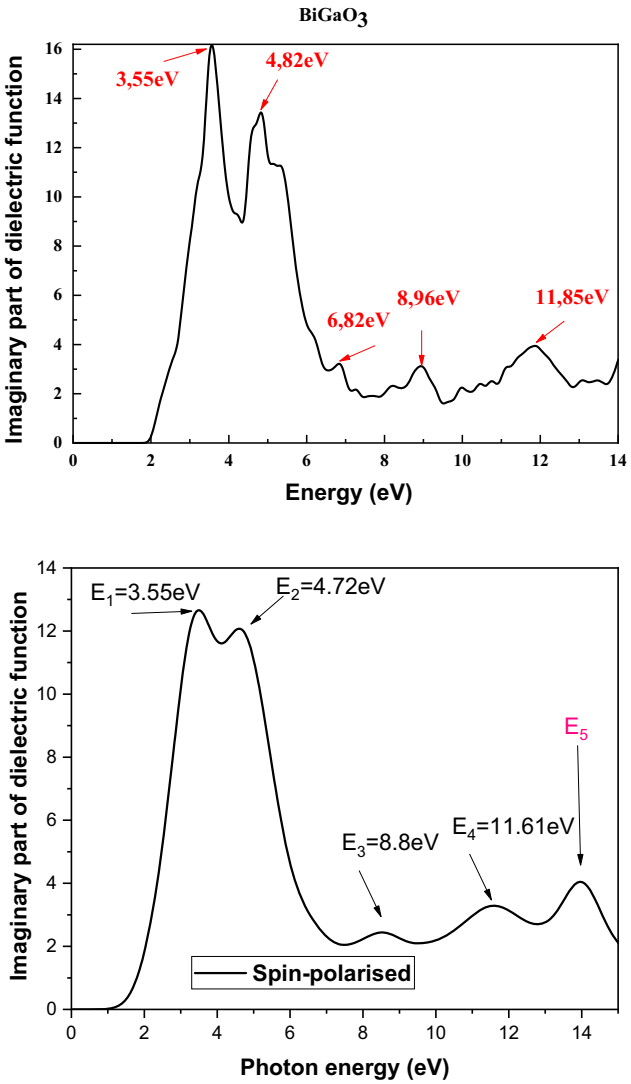

Figure 9. Effect of photon energy on imaginary part of the dielectric function with and without spin-polarized effect.

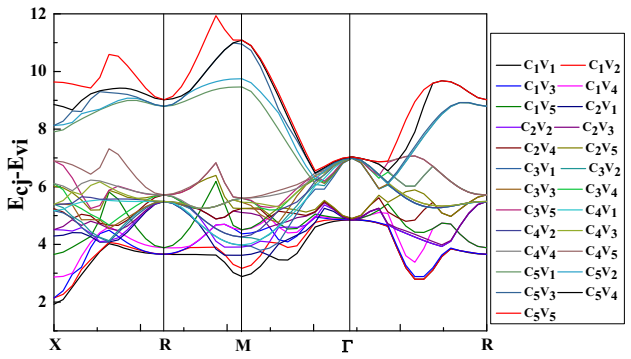

Figure 10. The transition energy $E_{cj} - E_{vi}$.

ultraviolet light irradiation. The high value of absorption with spin-polarized and without spin-polarized is 453302 cm^{-1} and 350000 cm^{-1} at wavelength 44.8 nm. The high

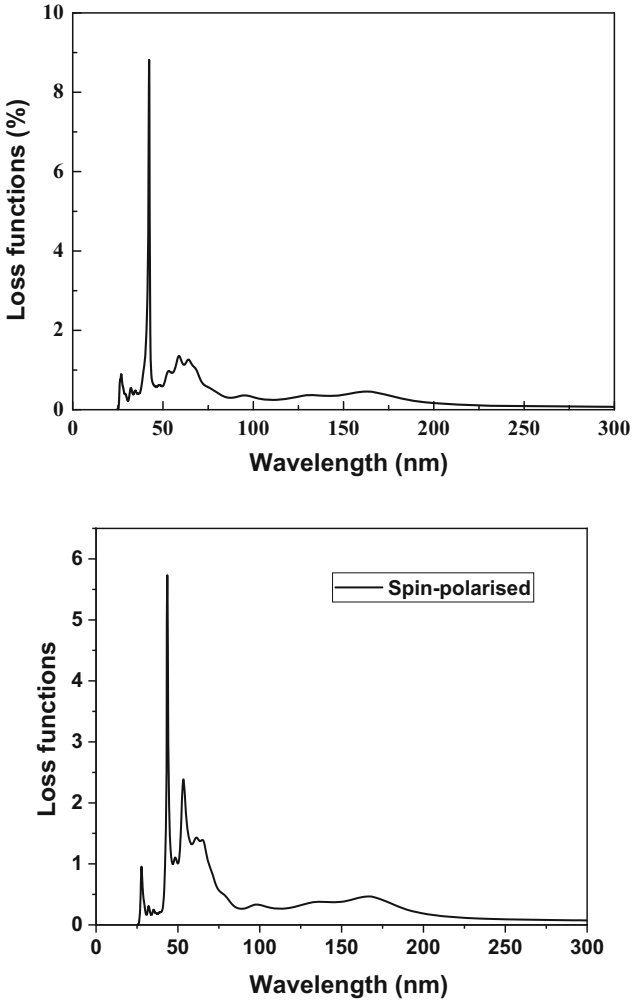

Figure 11. The loss function as a function of wavelength with and without spin-polarized effect.

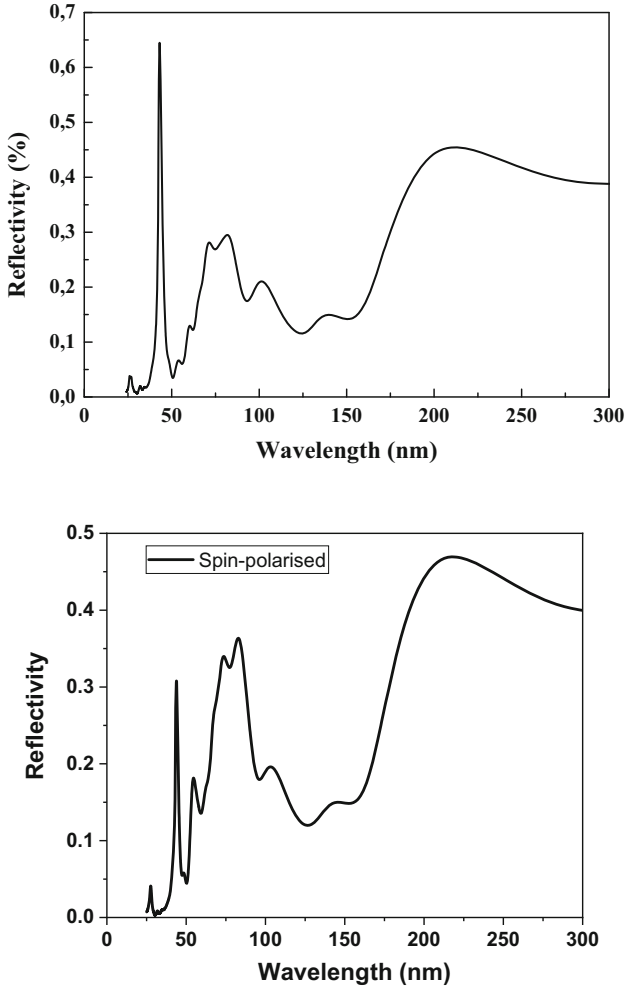

Figure 12. The reflectivity *vs.* wavelength with and without spin-polarized effect.

absorption value indicates that $BiGaO_3$ is candidate as a photocatalyst.

3.7 *Thermodynamic properties*

We study the effect of temperature and pressure on thermodynamic parameters of $BiGaO_3$. We carried out total energy *vs.* unit cell volume. Thermal parameters are determined in temperature and pressure ranging from 0 to 1800 K and 0−50 GPa. We note that Debye model indicates that heat capacity is proportional to T^3 at low temperature and follows Dulong–Petit law at high temperature. Figure 14 shows the effect of temperature on unit cell volume. The volume increases (decreases) when temperature (pressure) is enhanced. At 300 K and zero pressure, the lattice constant is 3.6728 Å. Figure 15 shows the temperature effect on bulk modulus. The compressibility decreases (increases) with increasing temperature (pressure). At 300 K and zero pressure, the compressibility is 170.13 GPa. Figure 16 displays the effect of temperature on Debye temperature. Debye temperature is substantially constant between 0 and 300 K, and then follows a linear decrease. We notice that Debye temperature is enhanced under pressure effect. At 300 K and zero pressure, θ_D is 457.34 K, which is closer to that estimated by elastic constants within GGA. We plot in figure 17 the effect of temperature on volumetric thermal expansion coefficient. We show that α increases sharply up to 500 K; then it follows the linear increase. At T = 300 K and P = 0 GPa, α is 2.93 × 10^5 K^{-1}. At high temperature, C_V tends to the Dulong–Petit limit [45], while at low temperature, it is proportional to T^3 [46]. Figures 18 and 19 represent the effect of temperature on C_V and C_P. From 0 to 500 K, C_V and C_P increase exponentially and the difference between them is very low. At high temperature (T > 500 K), C_P follows a linear increase whereas C_V tends to Dulong–Petit limit. At high temperature, C_V tends to approach 122.79 J mol^{-1} K^{-1}. At zero pressure and ambient temperature, C_V and C_P are 111.34 J mol^{-1} K^{-1} and

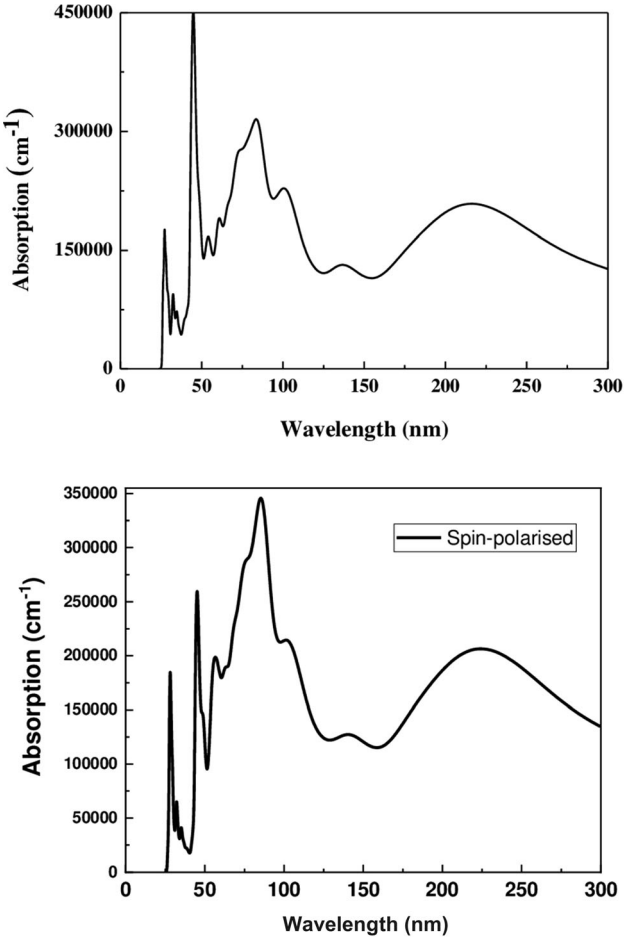

Figure 13. The absorption *vs.* wavelength with and without spin-polarized effect.

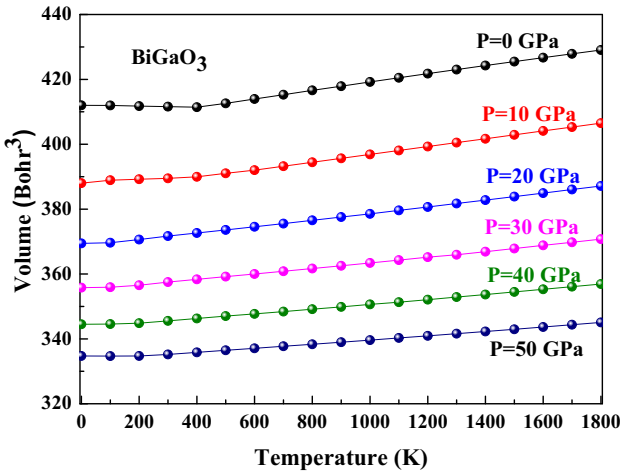

Figure 14. The volume–temperature diagram of $BiGaO_3$.

111.34 mol^{-1} K^{-1}. Figure 20 represents the dependence on temperature and pressure of theoretical entropy *S*. The shape of the curve is exponential. At zero pressure and 300 K, the entropy is 120.66 J mol^{-1} K^{-1} for $BiGaO_3$.

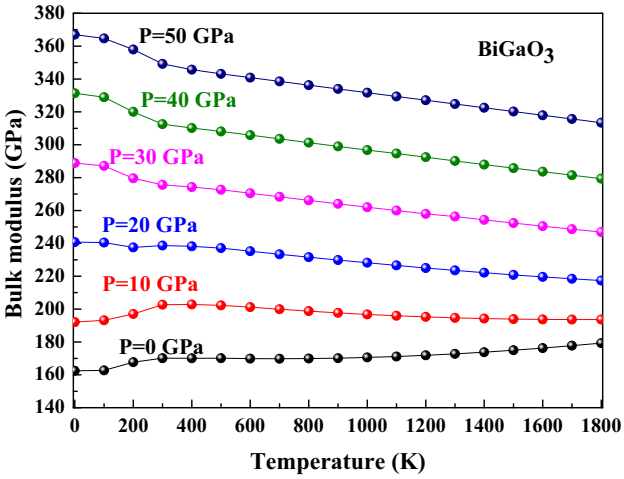

Figure 15. The bulk modulus *vs.* temperature for $BiGaO_3$.

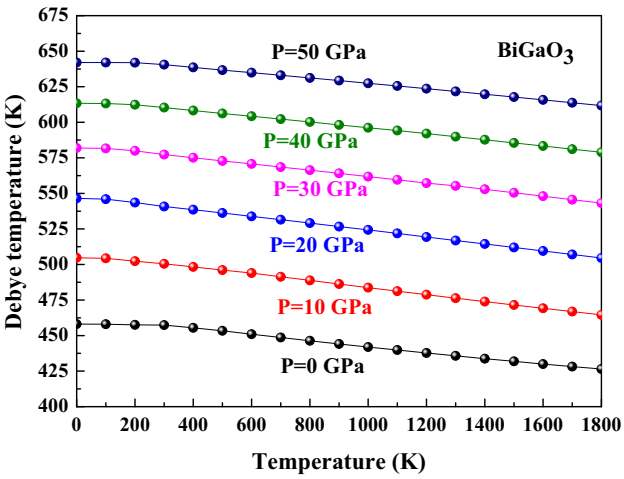

Figure 16. Effect of temperature on Debye temperature for $BiGaO_3$.

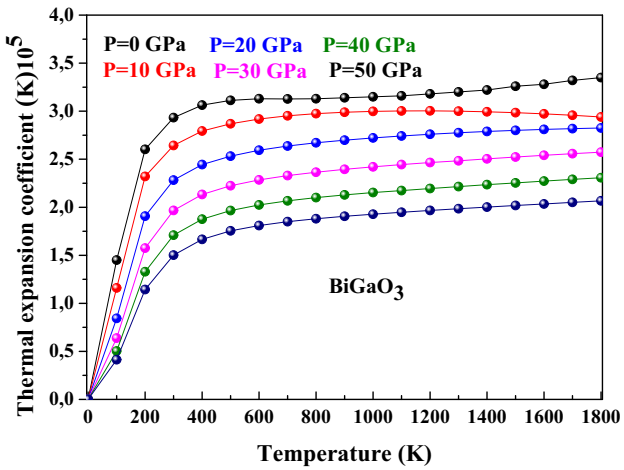

Figure 17. The volumetric expansion coefficient *vs.* temperature.

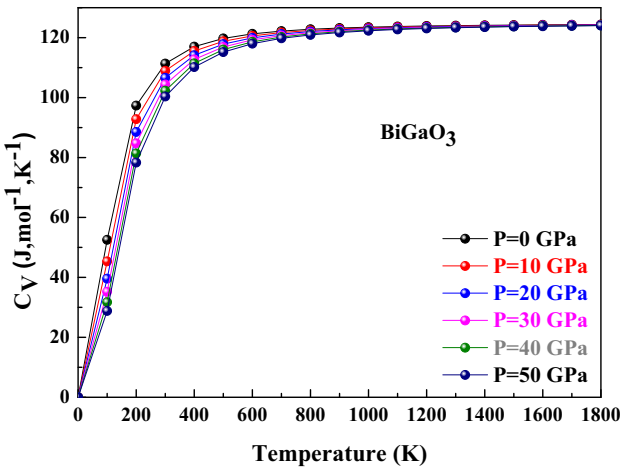

Figure 18. Effect of temperature on constant volume heat capacity C_V.

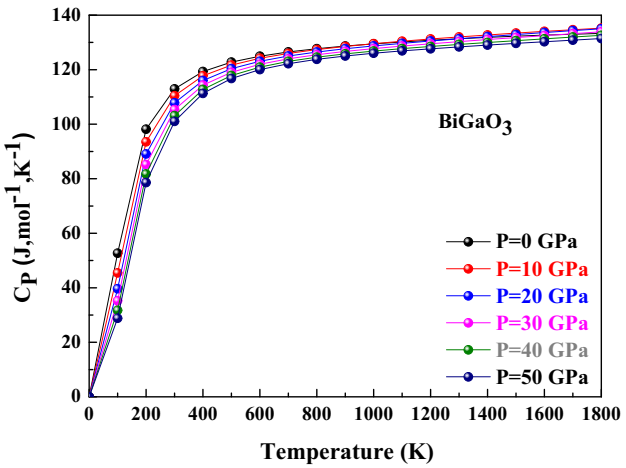

Figure 19. Effect of temperature on constant pressure heat capacity C_P.

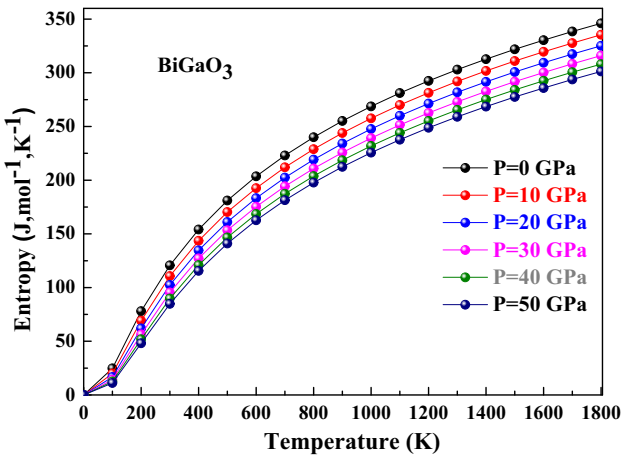

Figure 20. Effect of temperature on entropy S.

Table 6. Predicted constant pressure heat capacity, constant volume heat capacity and entropy for $BiGaO_3$.

Temperature (K)	C_P (J mol^{-1} K^{-1})	C_V (J mol^{-1} K^{-1})	S (J mol^{-1}K^{-1})
0	0	0	0
100	52.67	52.55	24.72
200	98.15	97.32	78.02
300	112.95	111.34	120.66
400	119.33	116.99	154.05
500	122.77	119.73	181.03
600	124.95	121.26	203.64
700	126.50	122.19	223.04
800	127.69	122.79	240.03
900	128.66	123.21	255.13
1000	129.48	123.50	268.74
1100	130.18	123.72	281.11
1200	130.80	123.89	292.47
1300	131.36	124.01	302.96
1400	131.84	124.12	312.72
1500	132.28	124.20	321.83
1600	132.66	124.26	330.39
1700	133.01	124.32	338.44
1800	133.30	124.36	346.057

The predicted C_V, C_P and and S for $BiGaO_3$ are listed in table 6 using GGA.

4. Conclusion

$BiGaO_3$ was studied by PP-PW method of the density functional theory within GGA and LDA approaches. The equilibrium lattice constant and bulk modulus are closer to the theoretical one. Elastic moduli as a function of pressure follow a linear increase. Shear and Young's moduli, Poisson's ratio, average sound velocities and Debye temperature are estimated in the framework of Voigt-Reuss-Hill approximations. $BiGaO_3$ material is a potential candidate as photocatalyst. Bi-6p state in the conduction band minima confirms that Bi-O bond has ionic bonding. Threshold energy of dielectric function corresponds to the fundamental indirect band gap for $BiGaO_3$. We predicted constant pressure and volume heat capacities and entropy using GGA functional for $BiGaO_3$. The effect of temperature and pressure on volume, bulk modulus, Debye temperature, volumetric thermal expansion coefficient, constant volume heat capacity, constant pressure heat capacity and entropy was investigated for the first time. We determined the lattice constant, bulk modulus, Debye temperature, the volumetric thermal expansion coefficient, C_V, C_P and S at 300 K and equilibrium pressure.

Acknowledgements

We acknowledge Taif University Research Supporting Project number (TURSP-2020/63), Taif University, Taif, Saudi Arabia.

References

[1] Cheong S W and Mostovoy M 2007 *Nat. Mater.* **6** 13
[2] Belik A A 2012 *J. Solid State Chem.* **195** 32
[3] Caracas R and Cohen R E 2007 *Appl. Phys. Lett.* **91** 093901
[4] Hill N A and Rabe K M 1999 *Phys. Rev. B* **59** 8759
[5] Seshadri R and Hill N A 2001 *Chem. Mater.* **13** 2892
[6] Kaczkowski J and Jezierski A 2013 *Acta Phys. Pol. A* **124** 852
[7] Kourdassi A, Benkhettou N, Labair M, Benkabou M, Benalia S, Khenata R *et al* 2014 *Braz. J. Phys.* **44** 914
[8] Kaczkowski J 2014 *J. Alloys Compd.* **613** 175
[9] Li C, Wang B, Wang R, Wang H and Lu X 2008 *Comput. Mater. Sci.* **42** 614
[10] Basith M A, Kurni O, Alam M S, Sinha B L and Ahmmad B 2014 *J. Appl. Phys.* **115** 024102
[11] Belik A A, Iikubo S, Kodama K, Igawa N, Shamoto S and Niitaka S 2006 *Chem. Mater.* **18** 798
[12] Zhang J Z, Ding H C, Zhu J J, Li Y W, Hu Z G, Duan C G *et al* 2014 *J. Appl. Phys.* **115** 083110
[13] Belik A A, Stefanovich S Y, Lazoryak B I and Takayama-Muromachi E 2006 *Chem. Mater.* **18** 1964
[14] Lee M H, Kim D J, Choi H I, Kim M, Song T K, Kim W J *et al* 2019 *ACS Appl. Electron. Mater.* **1** 1772
[15] Yang T, Wang Y, Fan L, Wang N, Lin K, Chen J *et al* 2020 *J. Phys. Chem. C* **124** 20445
[16] Akram F, Malik R A, Khan S A, Hussain A, Lee S, Lee M H *et al* 2018 *J. Electroceramics* **41** 93
[17] Kaczkowski J 2016 *J. Mater. Sci.* **51** 9761
[18] Lee M K, Bu S D and Lee G J 2019 *Energies* **12** 103390
[19] Segall M D, Lindan P J D, Probert M J, Pickard C J, Hasnip P J, Clark S J *et al* 2002 *J. Condens. Matter. Phys.* **14** 2717
[20] Hohenberg P and Kohn W 1964 *Phys. Rev. B* **136** 864
[21] Kohn W and Sham L J 1965 *Phys. Rev. A* **140** 1133
[22] Vanderbilt D 1990 *Phys. Rev. B* **41** 7892
[23] Perdew J P, Burke K and Ernzerhof M 1996 *Phys. Rev. Lett.* **77** 3865
[24] Goedecker S, Teter M and Hutter J 1996 *Phys. Rev. B* **54** 1703
[25] Monkhorst H J and Pack J D 1976 *Phys. Rev. B* **13** 5188
[26] Fischer T H and Almlof J 1992 *J. Phys. Chem. B* **96** 9768
[27] Blanco M A, Francisco E and Luaña V 2004 *Comput. Phys. Commun.* **158** 57
[28] Blanco M A, Pendás A M, Francisco E, Recio J M and Franco R 1996 *J. Mol. Struct. Theochem.* **368** 245
[29] Flórez M, Recio J M, Francisco E, Blanco M A and Pendás A M 2002 *Phys. Rev. B* **66** 144112
[30] Francisco E, Recio J M, Blanco M A and Pendás A M 1998 *J. Phys. Chem. B* **102** 1595
[31] Francisco E, Blanco M A and Sanjurjo G 2001 *Phys. Rev. B* **63** 049107
[32] Ghebouli M A, Chihi T, Ghebouli B and Fatmi M 2018 *Chin. J. Phys.* **56** 323
[33] Behram R B, Iqbal M A, Alay-e-Abbas S M, Sajjad M, Yaseen M, Arshad M I *et al* 2016 *Mater. Sci. Semicond. Process.* **41** 297
[34] Huntington H B 1947 *Solid State Phys.* **8** 60553
[35] Voigt W 1928 *Lehrbuch der Kristallphysik, Teubner, Leipzig*
[36] Reuss A 1929 *Z. Angew. Math. Mech.* **9** 49
[37] Hill R 1952 *Proc. Phys. Soc. A* **65** 349
[38] Gencer A and Surucu G 2018 *Mater. Res. Express.* **51** 51080478
[39] Mattesini M, Magnuson M, Tasnádi F, Höglund C, Abrikosov I A and Hultman L 2007 *Phys. Rev. B* **75** 129901
[40] Anderson O L 1997 *J. Phys. Chem. Solids* **58** 335
[41] Schreiber E, Anderson O L and Soga N 1973 *Elastic constants and their measurements* (New York:McGraw-Hill)
[42] Ghebouli M A, Ghebouli B, Zeghad A, Chihi T, Fatmi M and Ahmed S I 2021 *J. Mater. Res. Sci. Tech.* **14** 1958
[43] Li D, Ling F, Zhu Z and Zhang X 2011 *Phys. B Condens. Matter* **406** 3299
[44] Fang Y, Kong X, Wang D, Liu J and Cui D 2019 *J. Phys. Chem. Solids* **127** 107114
[45] Dar S A, Srivastava V, Sakalle U K and Parey V 2018 *Eur. Phys. J. Plus* **133** 64
[46] Chen Z, Zhang X, Lin S, Chen L and Pei Y 2018 *Natl. Sci. Rev.* **5** 333